

# Analysis of SAXS Fiber Patterns by Means of Projections

N. Stribeck

Institut für Technische und Makromolekulare Chemie,  
Universität Hamburg, 20146 Hamburg, Germany

Results of two methods for the quantitative analysis of two-dimensional (2D) small-angle X-ray scattering (SAXS) patterns with fiber symmetry are presented. Experimental data originate from studies of poly(ether ester) (PEE) thermoplastic elastomer materials recorded during straining experiments at a synchrotron beamline. The first steps of both methods are similar. By suitable projection of the 2D image data onto a line (longitudinal scattering, first method) or onto a plane (transverse scattering, second method) scattering curves are extracted, which finally can be analyzed in terms of two-phase structural models considering soft domains and hard domains inside the PEE. The studied longitudinal scattering in principal is one-dimensional and originates from chords crossing the soft and hard domains parallel to the direction of strain only. From these curves interface distribution functions (IDF) are computed and analyzed using an advanced stacking model. Not only the average domain heights, but four parameters characterizing each of two height distributions (hard and soft domains) are determined as a function of elongation. With several PEE materials strong equatorial scattering is observed during elongation. The equatorial scattering is similar to the frequently discussed void scattering but originates from an ensemble of rodlike soft domains (needles) in the sample, oriented parallel to the direction of strain. It can be studied using the second method. From the transverse scattering the 2D chord distribution is computed, from which the diameter distribution of the soft needles can be extracted. It is investigated as a function of strain.

## Introduction

If structural transformations shall be investigated, which occur during manufacturing or processing of polymer materials, one can only use those few methods which are non-destructive and do not interfere with the process itself. In this field scattering methods belong to the most powerful ones. Scattering theory promises the experimenter that he should be able to quantify a wide range of structural parameters, if only the data are recorded with sufficient accuracy. Among these parameters are size and distribution of domains in a multi-phase material, which can be studied using small-angle X-ray scattering (SAXS). Utilizing a powerful source (synchrotron beam) and a high resolution two-dimensional detector, nowadays it becomes possible to record series of detailed scattering patterns with high accuracy during short exposure time.

This chapter presents an overview of work that has been performed by the author aiming to develop adapted (i. e. a structural model is chosen as late as possible) evaluation methods for SAXS diagrams with fiber symmetry and the results obtained so far [1–4]. The basic principle of the methods to be presented is the extraction of curves from the 2D data in the scattering patterns by certain kinds of integrations (“projections”). The importance of such projections has early been recognized [5]. Novel is the analysis of the extracted curves in terms of 1D and 2D structural models. Applicability is assessed by comparison of the results with the obvious features of the scattering images.

## Experimental

### Materials

Poly(ether ester)s (PEE) are common thermoplastic elastomers exhibiting a two-phase structure of hard domains in a soft matrix. They can frequently be found in automobiles and as tube materials. Two kinds of multiblock PEEs are investigated. In the first group the soft segment blocks are made from poly(ethylene glycol) (PEG). The second group of samples is made from material in which the soft segment blocks consist of poly(tetrahydrofuran) (PTHF). Hard segment blocks of all samples are made from poly(butylene terephthalate) (PBT). Soft segment block lengths are in the order of magnitude of 1000 g/mole. Experiments have been carried out for materials with the hard segment ratio ranging from 35 % to 60 %. Evaluated data presented here originate from experiments on materials with a hard segment content close to 60 %.

When such materials are quenched from the melt, they undergo phase separation forming hard and soft domains. Because phase separation is imperfect, it is common notion that considerable amounts of hard segments reside in soft domains and even the hard domains may contain some soft segments ( fig 1). Otherwise one would not be able to explain the observed domain sizes.

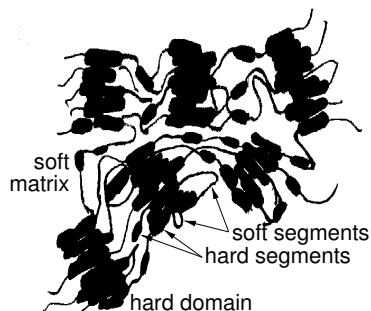


Figure 1. Discrimination between first, hard segment and hard domain and, second, between soft segment and soft domain (matrix).

### The Experiment

Straining and relaxation experiments are carried out in the synchrotron beam at HASYLAB in Hamburg, beamline A2. A typical maximum elongation  $\epsilon = (\ell - \ell_0)/\ell_0 \approx 3$  can be reached before the sample slips out of the clamps. During straining small-angle X-ray scattering patterns are recorded on image plates placed 1.8 m behind the sample. After exposing for 1 min the maximum recorded scattering intensity amounts to 60,000 counts. The geometry of the chosen semi transparent beam stop ensures low scattering background at the expense of a relatively large central blind area.

Data analysis is carried out using published computer programs[1], which are freely available[6].

## Evaluation Methods

### Basic Definitions and General Concept

Because all the samples exhibit a scattering pattern with fiber symmetry, it is convenient to write the intensity  $I(\vec{s}) = I(s_{12}, s_3)$  in cylindrical coordinates, with  $s_{12} = \sqrt{s_1^2 + s_2^2}$  and the component  $s_3$  defining the symmetry axis of the pattern. Let the magnitude of the scattering vector be defined by  $|\vec{s}| = (2/\lambda)\sin\theta$ , with  $\lambda$  being the wavelength of radiation and  $2\theta$  the scattering angle. Because the validity of the tangent plane approximation can be assumed, the complete information of SAXS is in a two-dimensional (2D) pattern. Such patterns may exhibit many reflections, which moreover may vary considerably as a function of tunable parameters (fig 3). Thus the analysis of a 2D pattern appears to be cumbersome because of the wealth of data. But for a 2D image there do exist several methods to extract specific information. Curves gained by such a procedure only reflect certain aspects of the morphology, and thus hopefully can be described by a simple structural model.

First steps towards this goal have been undertaken by Bonart [5]. Based upon the

mathematical relation between structure and scattering, he has proposed to analyze projections, which can be extracted from the scattering patterns and reflect a longitudinal and a transverse structure, respectively. Following a concept of Ruland [7, 8], the resulting curves are not fitted by a complex model, but analyzed step by step in order to “peel off” information. Finally a chord distribution[9] or an interface distribution[10] is computed. Only now, based upon the observed properties of the resultant distribution, an adapted model is chosen.

### Projections of Fiber Patterns

#### *Definitions of Special Projections*

Projections are integral operators which map functions onto subspaces of their definition domain. They shall be denoted by a pair of curly parentheses. The best known projection in the field of scattering theory maps the scattering intensity  $I(\vec{s})$  onto a zero-dimensional subspace, which is the number  $Q$ , known as “invariant” or “scattering power”

$$\{I\}_0 = Q = \int I(\vec{s}) d^3s. \quad (1)$$

Bonart’s longitudinal structure is obtained by not integrating over the whole reciprocal space, but only over planes normal to the fiber axis yielding a curve

$$\{I\}_1(s_3) = 2\pi \int_0^\infty s_{12} I(s_{12}, s_3) ds_{12} \quad (2)$$

which is a function of  $s_3$  only. Thus we identify this curve as a projection onto a one-dimensional subspace and indicate this by subscripting to the pair of braces. Analogously Bonart’s transverse structure

$$\{I\}_2(s_{12}) = 2 \int_0^\infty I(s_{12}, s_3) ds_3 \quad (3)$$

is computed by integrating along lines running parallel to the direction of strain. In the case of fiber pattern symmetry, this projection can be displayed as a curve. Nevertheless we should bear in mind that it is defined over a two-dimensional domain, the  $s_{12}$ -plane. Because, in principal, all these integrals have to be extended to infinity, one should take care to register the scattering intensity over a wide angular range.

#### *Projections and Sections*

Because of a general theorem of Fourier transformation theory, projections in reciprocal space are equivalent to sections in physical space (fig 2). But what is the definition of a section? In this review it may be allowed to explain the idea of a section intuitively.

Every scientist who has investigated fiber patterns, has placed sections in measured images. E. g., he studies the scattering intensity along a straight line extending from the center of the pattern out through the maximum of a reflection. Exactly this is a section of the scattering intensity. Not rarely such section is placed in a manner that it includes

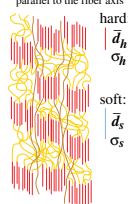
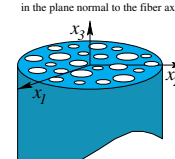
Intensity projection	Physical space section - structural meaning
$\langle I_1 \rangle = Q$	$\phi_h (1 - \phi_h) \Delta \rho_{el}^2$ Non-topological character of the two-phase system
$\langle I_1 \rangle_{(s_3)}$	1-dimensional two-phase system parallel to the fiber axis  Domain height distributions (hard, soft)
$\langle I_2 \rangle_{(s_2)}$	2-dimensional two-phase system in the plane normal to the fiber axis  Chord distribution (needle, matrix)

Figure 2. Relations between some intensity projections and corresponding structural features in physical space for the case of SAXS from fibers. (Reproduced with permission from reference [2] © 1999 ACS)

an angle  $\varphi$  with the fiber direction. Intuitive reasoning now may lead to the erroneous conclusion that the variation of scattering intensity along the chosen line would describe the correlations (of, e. g. domains) in the chosen direction. But on account of the above mentioned Fourier theorem, the shape of the curve only describes the projection of deliberately oriented correlations onto the chosen direction of the cut. This projection is carried out not in the reciprocal space depicted by the fiber pattern, but in the physical space of the materials structure. Projection in physical space is hard to imagine and, consequently, it can hardly be described by a structural model. Only in the special case of a structure generated from stacks of flat and extended lamellae [8, 9, 11–17], the intensity found in a section can easily be related to structural notions. Then the well-known “Lorentz correction” is practically applied to isotropic scattering patterns, and it performs similar transformation as does a projection to fiber axis in the case of fiber patterns: It extracts a scattering curve related to a *section* through a one-dimensional structure *in physical space* from a scattering pattern.

Objections against an analysis of intensity projections are heard from time to time. Argumentation is based on intuitive reasoning and avoids to make use of scattering theory. The most frequent objection tells that a projection of the intensity “doubtlessly smears the details” of information which are present in the 2D scattering pattern. Behind this reasoning is the feeling that information gets lost. But the same, of course, is valid when a section of the scattering pattern is analyzed. Moreover, by common understanding materials structure is preferably described in physical space, and only intensity

projection guarantees that no “smearing of structural details” in physical space must be taken into account when the structural model is built.

A second objection starts from the correct finding that different fiber diagrams (“four- and two-point diagrams”) may result in identical projected intensities. This objection is not well-founded, since it is based on the erroneous implication that projection analysis would claim to fully characterize oriented structures. By contrast, intensity projection analysis studies intersections of the correlation function, and if two structures result in the same projected intensity with respect to fiber axis, they indeed share the same intersection of their correlation functions with respect to the fiber direction. Consequently, after projection it is allowed to describe a four-point pattern and a two-point pattern by the same one-dimensional mathematical model of alternating domains.

Although misorientation of lamellar stacks or fibrils will have significant effects on scattering pattern and structure, such effects do not affect the applicability of the method of projection analysis, as long as one accepts that the aim of analysis is not the determination of layer thickness distributions, but the determination of distributions of chord lengths passing through layers in fiber direction only. And just this structural aspect of fiber structure, as to my belief, is the most important one to be related to materials performance. Falling back to the problem of misorientation, inclined layers will simply increase the fraction of longer chords in the resulting chord length distribution, because fiber direction cuts through such layers under an oblique angle. And if the domains are not shaped like layers or needles, the discussion of orientation is obsolete anyway. But now let us start to discuss the most important projections in SAXS fiber patterns.

#### *Invariant*

It is well-known that the invariant  $Q$  contains all information on the non-topological character of the structure. Thus, if the electron density difference  $\Delta\rho_{el}$  between hard domains and soft matrix is the predominant one, it may be possible to gain information on the volume fraction  $\phi_h$  of hard domains in the sample.

#### *Longitudinal Structure*

$\{I\}_1(s_3)$  is a one-dimensional scattering intensity which is related to the section  $[\gamma]_1(x_3)$  of the correlation function  $\gamma(\vec{x})$  in  $x_3$  direction. Thus it contains information only on those chords passing the two-phase system in the direction parallel to the fiber axis,  $x_3$ . On the right hand side of the middle row in fig 2 we may represent such a chord by a deliberate vertical line. Traveling along such a line, we will alternately move through the hard and the soft domain phase, from time to time crossing a phase boundary. Thus structural parameters of physical interest are  $\bar{d}_h$ , the average travel distance inside the hard domain phase,  $\bar{d}_s$ , the average travel distance inside the soft domain phase as well as the variances ( $\sigma_h$ , and  $\sigma_s$ ) of their distributions, which shall be called “domain height distributions”  $h_h(x_3)$  and  $h_s(x_3)$ .

Thus by computing the longitudinal structure we eliminate all information on transverse correlation of domains from the scattering pattern and reduce the problem to the case of one-dimensional scattering curves, which is well-known from the theory of lamellar two-phase systems. For the solution of the 1D problem appropriate data analysis methods are at hand [2, 8, 10, 15, 16]. As has been mentioned above, analysis of

isotropic samples with a lamellar domain structure and the analysis of longitudinal intensity projections are closely related to each other. In the first case a Lorentz correction ( $I_1(s_3) = 2\pi s_3^2 I(s_3)$ ;  $s_3 \equiv s$ ) and in the second case a projection (eq 2) both result in an intensity which is related to a *one-dimensional structure in physical space*. Thus after the extraction of the “1D intensity” analysis proceeds in the same way for both cases. While from a mathematical point of view the first method is only applicable for isotropic samples with a lamellar structure, the second is generally applicable. From the physical point of view the second method is favorably applied to well-oriented systems. Both kinds of 1D intensities share the same 1D Porod’s law falling off with  $s_3^{-2}$ , because they both are related to sections in physical space. Generally comparing projection analysis to an analysis of intensity sections, there is no dilemma concerning the expected fall-off of scattering intensity in the Porod region with projections even in the case of varying misorientation. Finally, the well-known dilemma with intensity sections is only a result of the unknown effect of projection in the space where the structure is.

#### *Transverse Structure*

If the pattern reveals equatorial scattering, the equatorial streak may be extracted from the pattern and analyzed separately. In certain cases (If the streak is clearly separated from other reflections and does not “fan out”) it should suffice to mask the measured pattern

$$I_n(s_{12}, s_3) = I(s_{12}, s_3) Y_b(s_3) \quad (4)$$

in order to extract a “needle scattering”,  $I_n(s_{12}, s_3)$ , in particular if this pattern shall only be interpreted after projecting it.  $Y_b(s_3)$  is a shape function, which gives a value of 1 for  $|s_3| < b/2$  and vanishes elsewhere. Thus  $b$  is the height of the equatorial band.

When dealing with the equatorial streak of a fiber pattern, it appears suitable to extract the transverse structure  $\{I\}_2(s_{12})$ . Through Fourier transformation relation this projection is linked to a two-dimensional two-phase system made from needle cross sections in a matrix, as indicated in the bottom row of fig 2.

#### *Evaluation of the Transverse Structure*

An adapted method for the evaluation of the transverse structure had to be developed[3].  $\{I\}_2(s_{12})$  is generated by a projection process identical to the one carried out by a Kratky camera. In particular  $\{I\}_2(s_{12})$  exhibits Porod’s law with the scattering falling off with  $s_{12}^{-3}$ . Small deviations from the predicted fall off are accounted to the non-ideal structure of the real two-phase system[7, 18] and corrected accordingly, leading to the 2D interference function  $G_2(s_{12})$  of an ideal two-phase system

$$G_2(s_{12}) = (\{I\}_2(s_{12}) - I_{Fl}) s_{12}^3 / \exp\left(-\frac{4}{9}\pi^2 w_t^2 s_{12}^2\right) - A_{P_2}. \quad (5)$$

$A_{P_2}$ , Porod’s asymptote of the projected SAXS intensity, is the constant governing Porod’s law. The non-ideal structure of the real two-phase system is described by  $I_{Fl}$  and  $w_t$ . Fluctuations of the electron density are considered by  $I_{Fl}$ , the density fluctuation background.  $w_t$  is the width of the transition zone at the domain boundary.

From  $G_2(s_{12})$  the 2D chord distribution [19, 20]  $g_2(x_{12})$  is computed by

$$g_2(x_{12}) = \pi \int_0^\infty (J_0(2\pi x_{12}s_{12}) - J_2(2\pi x_{12}s_{12})) G_2(s_{12}) ds_{12}. \quad (6)$$

Here  $J_0$  and  $J_2$  denote Bessel functions of the first kind. In general,  $g_2(x_{12})$  shows the distribution of chords from needle and matrix cross sections and their correlations in the plane normal to the fiber direction.

During the analysis of the experimental data it turned out that  $g_2(x_{12})$  is positive everywhere. Thus the correlations among the “disks in the plane” are negligible and  $g_2(x_{12})$  represents the chord distribution of an ensemble of uncorrelated disks in the  $(x_1, x_2)$ -plane (fig 2). Following the principle of late modeling, now it appears reasonable to model the cross section of every needle by a circular disk and to ask for the properties of a needle diameter distribution,  $h_D(D)$ .  $g_2(x_{12})$ , can be expressed in terms of  $h_D(D)$  and the intrinsic chord distribution  $g_c(x_{12})$  of a disk with unit diameter

$$g_2(x_{12}) = \int_0^\infty h_D(D) g_c\left(\frac{x_{12}}{D}\right) \frac{dD}{D} \quad (7)$$

is simply the superposition of compressed and expanded images from  $g_c$  weighted by the value of the diameter distribution,  $h_D(D)$ , which shall be studied. Eq 7 is the definition of the Mellin convolution [8, 21].  $h_D(D)$  can be computed by numerical inversion of eq 7 utilizing an iterative van Cittert algorithm similar to the one proposed by Glatzer[22]. Beyond that one can take advantage of special properties of the Mellin convolution and compute parameters characterizing the needle diameter distribution directly from the measured chord distribution utilizing moment arithmetics[3].

## Results and Discussion

### Principal SAXS Patterns of PEE

Images of many different grades of PEE have been recorded. Quantitative evaluation of the full set of data is still in progress. Four different classes of scattering patterns can be observed with these samples, which correspond to different basic structure and can be arranged in the order of increasing elongation (fig 3). None of the materials passes through all four states. E. g. the commercial material Arnitel E2000/60 (DSM, The Netherlands) only shows the “microfibrillar state” and the “soft needle state”. For this material the evaluation of the transverse structure has been carried out. The PEE 1000/57 from the laboratory of Fakirov, University of Sofia, on the other hand, starts from the “macro lattice state”, transforms into a “microfibrillar structure” and slips from the clamps thereafter. Data from this sample is used to demonstrate the evaluation of the longitudinal structure.

In the uppermost image of fig 3 one observes a scattering pattern with narrow beams of intensity, inclined with respect to the fiber axis. On these beams first and second order of the long period reflection can clearly be detected. Thus the structure can appropriately be described by stacks of tilted lamellae.



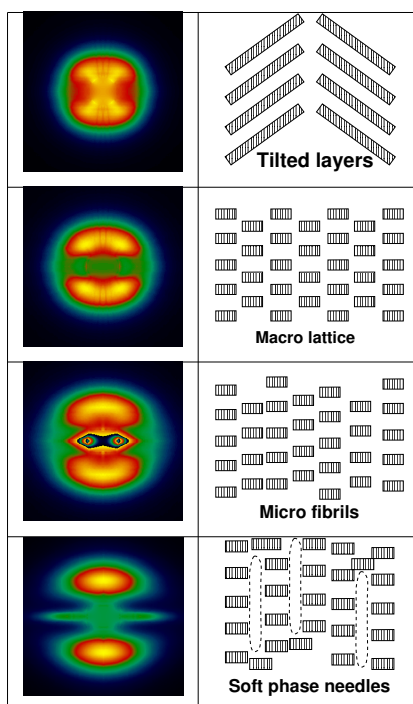


Figure 3. Typical SAXS patterns from various PEE samples under strain. Elongation increases from top to bottom.

The second state shows indented layer line reflections (“4–point–pattern”), the most appropriate model for which is that of a macro lattice[23, 24] from arranged microfibrils. Frequently one observes the shoulder of a second long period, which is not indented at the meridian (5th and 6th point), and has been attributed to slack microfibrils which do not respond to external strain any more[25] (fig 4). Both structural features are collected in a single intensity projection. This superposition may be considered a “smearing”. It will be demonstrated that nevertheless the chosen structural model is able to discriminate between both components in the projected data and to return structural data of each when used for fitting. Here the question of how to avoid superposition of multiple components in the projection arises, but let us discuss this issue in the Conclusions section.

### Analysis of the Longitudinal Structure

#### General Evaluation Steps

Projections of the SAXS pattern data from sample PEE 1000/57 according to eq 2 yield the scattering curves shown in fig 5(a). From these curves interface distribution functions (IDF) (fig 5(b)) are computed by use of eqs 5 and 6.

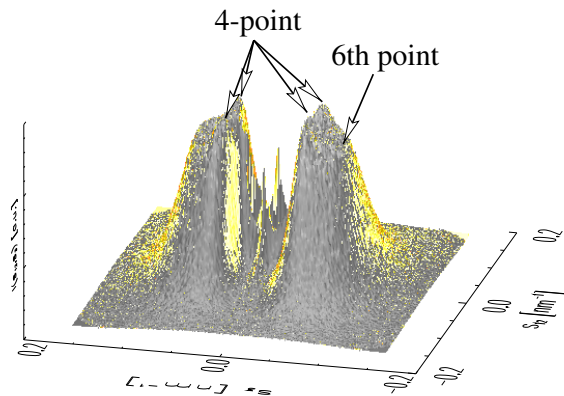


Figure 4. SAXS pattern of PEE 1000/57 at an elongation  $\epsilon = 0.88$ . The two different long periods are indicated by arrows emerging from two different labels. (Reproduced with permission from reference [2] © 1999 ACS)

In the final step of data evaluation these curves are fitted using a one-dimensional model function, which unifies[14] the two most frequently discussed models for one-dimensional statistics, namely stacking statistics[26] and “homogeneous long period distribution”[27, 28]. It turns out that whenever in the original scattering patterns a second long period is observed (fig 4), a fit is only possible if a two-component model is used. This fact is demonstrated in fig 6.

Thus in the end the longitudinal scattering of every one-component sample is described by two domain height distributions,  $h_h(x_3)$  and  $h_s(x_3)$ . Altogether both domain height distributions, in turn, are defined by a set of six parameters, namely the integral of the IDF,  $W$ ; the average domain heights of the hard and the soft domain phase, respectively,  $\bar{d}_h$  and  $\bar{d}_s$ ; the relative variances of the domain height distributions,  $\sigma_h/\bar{d}_h$  and  $\sigma_s/\bar{d}_s$ ; and finally the heterogeneity or skewing parameter,  $\sigma_H$ . Consequently a fit of a two-component sample yields values for 12 parameters. Now suitable visualizations of these parameters as a function of elongation  $\epsilon$  should help to gain better understanding of the structural changes during sample straining.

#### Domain Heights Determined from Longitudinal Structure

A plot of the average domain heights as a function of elongation  $\epsilon$  is shown in fig 7(a). Although in principal the assignment of soft and hard domain heights is ambiguous, the interaction of the different domain height distributions with external strain gives enough information to identify each distribution uniquely. After this identification, as a first result the volume fraction of hard domains in the original sample,

$$\phi_h = \frac{\bar{d}_h}{\bar{d}_h + \bar{d}_s}, \quad (8)$$

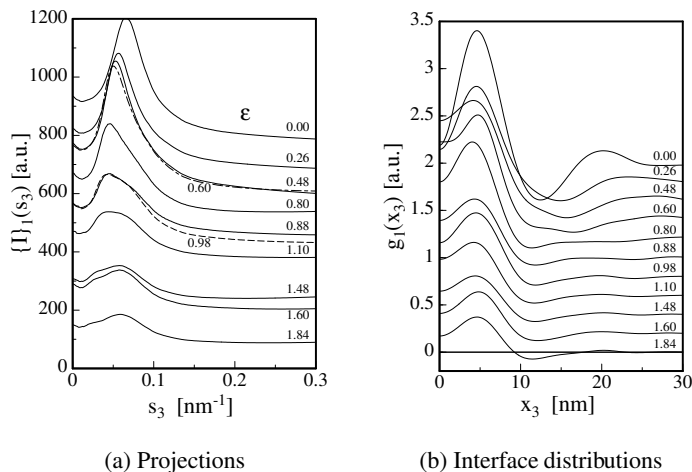


Figure 5. PEE 1000/57. (a) 1D scattering curves  $\{I\}_1(s_3)$  obtained by projection of scattering patterns onto the fiber direction. Curves are labeled with the elongation  $\epsilon$ . (b) IDFs  $g_1(x_3)$  from longitudinal scattering curves  $\{I\}_1(s_3)$ . (Reproduced with permission from reference [2] © 1999 ACS)

can be computed from its average hard domain height,  $\bar{d}_h = 7.4\text{nm}$ , and its average soft domain height,  $\bar{d}_s = 5.2\text{nm}$ . The computed value of  $\phi_h = 0.59$  is close to the hard-to-soft segment ratio of the polymer. Such agreement cannot be expected, since there are several structural features which have been discussed in literature in order to predict or to explain deviations. Nevertheless, data from an IDF analysis frequently result in such an agreement and this fact may become interesting to be studied.

At medium elongation we observe two kinds of microfibrils. The taut component (top in fig 7(a)) elastically interacts with the external strain, while the slack component (bottom in fig 7(a)) collects “garbage” from microfibrils, which are no longer connected to the surrounding elastic network and remain in the relaxed state.

At low elongations in the taut microfibrillar component soft domain heights start to grow continuously as a function of external elongation. The internal elongation of these soft domains is much higher than the externally applied elongation, which is a necessity because of the rigid nature of the hard domains filling the elastic network. Nevertheless, the average long period

$$L = \bar{d}_h + \bar{d}_s \quad (9)$$

of the taut component increases slower than external elongation  $\epsilon$ . This finding reflects the known fact that PEE polymers are far from an ideal elastic material. Pull out of taut tie-molecules from hard domains and a collapse of the hard domains observable at  $\epsilon = 0.8$  are characteristic for the straining process of such polymers. The quantitative data now gained from SAXS data analysis may serve to model the filled elastic network

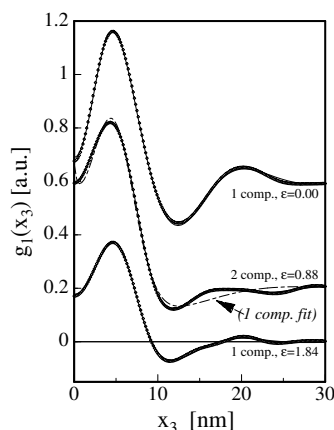


Figure 6. Model function fits to IDF's  $g_1(x_3)$ . Symbols marks represent data. Solid lines show the best fit. At medium elongation one observes two reflections in the scattering pattern and fitting requires a two-component model. (Reproduced with permission from reference [2] © 1999 ACS)

and finally to describe the material properties of both hard and soft domain phases.

Since not only average domain heights have been considered in the model function, the domain height distributions themselves can be reconstructed from the parameter values of the best fit. Examples for these height distributions are shown in fig 7(b). Here the height distributions  $h_h(x_3)$  of the hard domains in the taut microfibrillar component are presented. In the plot of the average domain heights we could hardly observe any change during the initial phase of straining. Watching the height distributions as a whole we now observe a narrowing, indicating that the domains with medium height are the most stable ones. By loss of tall and tiny hard domains to the slack component the height distribution narrows considerably. Thus a material with a narrow distribution of hard domain heights would probably be the more perfect elastomer.

Comprehensive discussion both of theoretical background and results can be found in the original paper[2].

## Analysis of the Transverse Structure

### General Evaluation Steps

For a straining series of the material Arnitel E2000/60 the equatorial scattering has been extracted and projected onto the transverse plane as discussed in the section "Evaluation Methods". The resulting curves of  $\{I\}_2(s_{12})$  are presented in fig 8(a). After proper consideration of the non-ideal two-phase structure of the sample[3] the 2D chord distribution  $g_2(x_{12})$  is computed by means of eq 6. The corresponding curves are shown in fig 8(b). When such equatorial scattering was first observed [29], it was attributed to

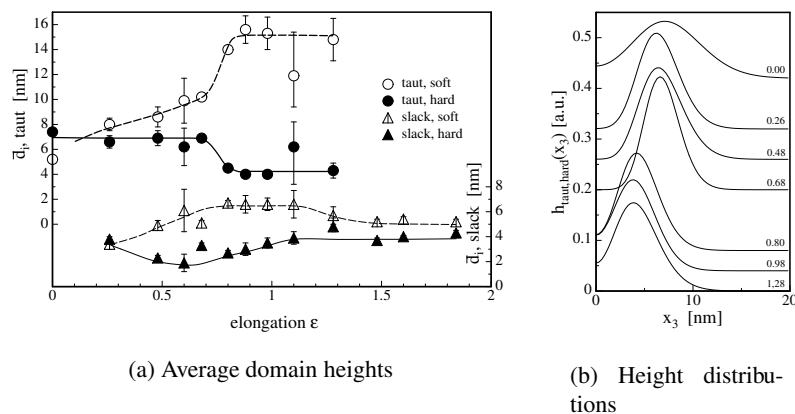


Figure 7. PEE 1000/57. (a) Average domain heights of taut (top, left scale) and slack (bottom, right scale) microfibrillar components as determined from fits. (b) Height distributions of the hard domains in the taut microfibrillar component as reconstructed from structural parameters determined in fits. (Reproduced with permission from reference [2] © 1999 ACS)

the existence of elongated microvoids in the fiber. Here, with the PEE samples, the formation of these elongated domains is preceded by the destruction of hard domains and growth of a long period reflection which merges with the primary beam before the equatorial scattering emerges. This peculiarity led to the interpretation that the observed equatorial scattering most likely is caused from elongated soft domains, which are a product of the destruction of hard domains. Those elongated soft domains thus should contain almost equal parts of soft and hard segments, according to the chemical composition of the poly(ester ether).

Because in good approximation the curves are positive everywhere, we are allowed to consider the structure to be built from an uncorrelated ensemble of domains, which shall be addressed as “soft needles”. Thus by application of moment arithmetics we compute the average needle diameter,  $\bar{D}$ , the relative width of the needle diameter distribution,  $\sigma/\bar{D}$  and the total cross section of the needles with respect to the total cross section of the fiber.

Data are presented in fig 9(a). From fig 9(a) it becomes obvious that the mean diameter of the needle shaped domains decreases almost linearly with increasing elongation, while for rubber elastic behavior, one would have expected a decrease according to  $\bar{D}(\epsilon) = \bar{D}_0/\sqrt{\epsilon+1}$ . As is shown in fig 9(b), the reason is that the disk diameter distribution alters its shape. With increasing elongation more and more thin needles are emerging, which cause the average diameter to decrease considerably. A different explanation for this effect can be given by an increasing raggedness of the needle cross sections circumferences. Extrapolating linearly towards  $\epsilon = 0$ , one finds a hypothetic average initial diameter  $\bar{D}_0 = 4.8$  nm of the soft domain needles.  $\sigma/\bar{D}(\epsilon)$ , the relative

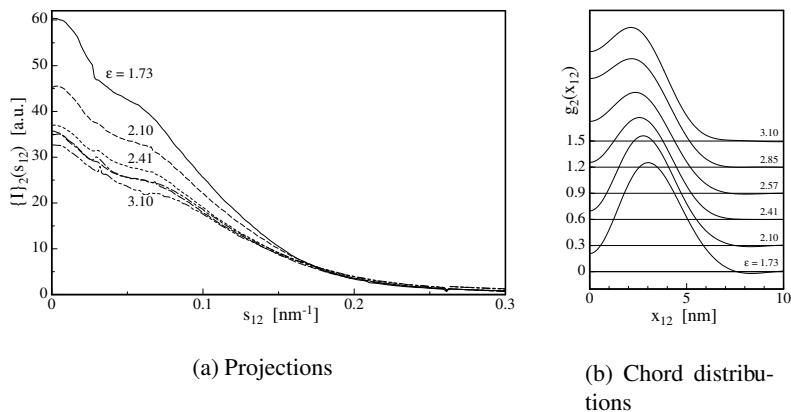


Figure 8. **a)** Projections  $\{I\}_2(s_{12})$  of the equatorial scattering onto the plane normal to straining direction. Arnitel E2000/60. **b)** Chord distributions  $g_2(x_{12})$  of Arnitel E2000/60 computed from the curves in (a). (Reproduced with permission from reference [3] © 1999 John Wiley.)

width parameter of the disk diameter distribution, hardly increases. The total needle cross section per fiber cross section, becomes constant for elongations  $\epsilon > 2.5$ . On the other hand, in the observable region of elongations  $1.7 < \epsilon < 2.5$  a considerable decrease is observed. This decrease indicates a strain hardening process of the soft needles: During the straining process the soft material of the needles is compressed in transverse direction with respect to the surrounding matrix material. An assumed increase of the needle density during this process would amplify the observed effect. The measured values could be compared with measurements of Young's modulus, and stress-induced polymorphic transitions[30] could be discussed in conjunction with the presented result. More comprehensive discussion of the theoretical background and the results can be found in the original paper [3].

## Conclusions

It has been demonstrated, how the utilization of the concept of projections can help to analyze two-dimensional SAXS patterns with fiber symmetry quantitatively. Because the computation of long ranging integrals is involved in this method, a prerequisite for successful analysis is the careful choice of a small beam stop, a wide vacuum tube, a rather short distance between sample and detector and a fast and linear detector. By doing so one can hope to register both all the reflections and also the important background scattering with required accuracy and spatial resolution.

Comparison of the determined structural parameters with the obvious features in a

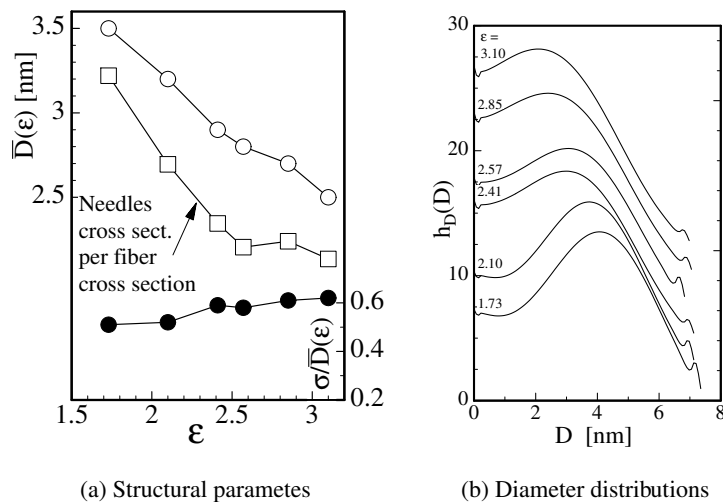


Figure 9. (a) Characterization of the ensemble of needle-shaped soft domains in Armitel E2000/60 as a function of elongation  $\epsilon$ . (b) Diameter distributions,  $h_D(D)$ , of soft domain needles computed by numerical Mellin deconvolution of curves shown in fig 8(b). (Reproduced with permission from reference [3] © 1999 John Wiley.)

series of scattering images shows good agreement. Therefore projection analysis appears to be a suitable method, if 2D scattering patterns with fiber symmetry shall be evaluated quantitatively. Both for the identification of structural components and for the purpose of testing the stability of the multi stage evaluation method, it helps to analyze a comprehensive data set, in which an external parameter like the elongation  $\epsilon$  is slowly varied. Thus one can obtain accurate quantitative data not only on domain size averages, but also on their statistics. All in all application of these methods results in a more detailed description of the domain structure from polymers in the oriented state.

If multiple structural components are obvious in the scattering patterns, one is tempted to separate the contributions directly in the scattering pattern. For the general case this idea is a considerable challenge, and it remains questionable if such an attempt would be successful without the necessity to sacrifice the principle of late structure modeling. A more promising approach, I believe, will be to transform the fiber diagram as a whole into a 3D chord distribution with fiber symmetry. By this operation no structural information is lost, but the information content of the scattering image will be transformed into physical space. In fact, the two kinds of chord distributions discussed in this work are nothing else but the two principal sections through this 3D chord distribution (in meridional and equatorial direction, respectively).

This investigation has been supported by the Bilateral Cooperation Program between the University of Hamburg and the University of Sofia, which is funded by the DAAD. SAXS investigations have been supported by HASYLAB Hamburg under project I-97-06. The study of the

Armitel material has kindly been suggested by Professor Kricheldorf, University of Hamburg. Sample material has been supplied by courtesy of DSM Corp., The Netherlands.

## Literature Cited

- [1] Stribeck, N. *Fibre Diffraction Rev.* 1997; 6, 20–24.
- [2] Stribeck, N.; Fakirov, S.; Sapoundjieva, D. *Macromolecules* 1999; *in print*.
- [3] Stribeck, N. *J. Polym. Sci., Part B: Polym. Phys.* 1999; *in print*.
- [4] Stribeck, N. *Proc. Am. Chem. Soc. PMSE Prepr.* 1998; 79, 393–394.
- [5] Bonart, R. *Kolloid Z. u. Z. Polymere* 1966; 211, 14–33.
- [6] Stribeck, N. *Web Page*. [www.chemie.uni-hamburg.de/tmc/stribeck/](http://www.chemie.uni-hamburg.de/tmc/stribeck/).
- [7] Ruland, W. *J. Appl. Cryst.* 1971; 4, 71–73.
- [8] Stribeck, N. *Colloid Polym. Sci.* 1993; 271, 1007–1023.
- [9] Méring, J.; Tchoubar-Vallat, D. *C. R. Acad. Sc. Paris* 1965; 261, 3096–3099.
- [10] Ruland, W. *Colloid Polym. Sci.* 1977; 255, 417–427.
- [11] Vonk, C. G. *Colloid Polym. Sci.* 1979; 257, 1021–1032.
- [12] Vonk, C. G.; Kortleve, G. *Kolloid-Z. u. Z. Polymere* 1967; 220, 19–24.
- [13] Ruland, W. *Colloid Polym. Sci.* 1978; 256, 932–936.
- [14] Stribeck, N. *J. Phys. IV* 1993; 3, 507–510.
- [15] Verma, R. K.; Velikov, V.; Kander, R. G.; Marand, H.; Chu, B.; Hsiao, B. S. *Polymer* 1996; 37, 5357–5365.
- [16] Verma, R.; Marand, H.; Hsiao, B. *Macromolecules* 1996; 29, 7767–7775.
- [17] Baltà Calleja, F. J.; Vonk, C. G. *X-Ray Scattering of Synthetic Polymers*. Elsevier, Amsterdam, 1989.
- [18] Stribeck, N.; Reimers, C.; Ghioca, P.; Buzdugan, E. *J. Polym. Sci., Part B: Polym. Phys.* 1998; 36, 1423–1432.
- [19] Tchoubar, D.; Méring, J. *J. Appl. Cryst.* 1969; 2, 128–138.
- [20] Schmidt, P. W. *J. Math. Phys.* 1967; 8, 475–477.
- [21] Marichev, O. I. *Handbook of Integral Transforms of Higher Transcendental Functions*. Ellis Horwood Ltd., Chichester, 1983.
- [22] Glatter, O. *J. Appl. Cryst.* 1974; 7, 147–153.
- [23] Fronk, W.; Wilke, W. *Colloid Polym. Sci.* 1983; 261, 1010–1021.
- [24] Fronk, W.; Wilke, W. *Colloid Polym. Sci.* 1985; 263, 97–108.
- [25] Stribeck, N.; Sapoundjieva, D.; Denchev, Z.; Apostolov, A. A.; Zachmann, H. G.; Stamm, M.; Fakirov, S. *Macromolecules* 1997; 30, 1329–1339.
- [26] Hermans, J. J. *Rec. Trav. Chim. Pays-Bas* 1944; 63, 211–218.
- [27] Stribeck, N.; Ruland, W. *J. Appl. Cryst.* 1978; 11, 535–539.
- [28] Strobl, G. R.; Müller, N. *J. Polym. Sci., Part B: Polym. Phys.* 1973; 11, 1219–1233.
- [29] Statton, W. O. *J. Polym. Sci.* 1962; 58, 205–220.
- [30] Apostolov, A. A.; Boneva, D.; Baltà Calleja, F. J.; Krumova, M.; Fakirov, S. *J. Macromol. Sci. - Phys.* 1998; 37, 543–555.